Journal of
Synchrotron
Radiation

ISSN 0909-0495

Received 23 October 2006
Accepted 11 May 2007

Determination of the magnetic spin direction from the nuclear forward-scattering line intensities

R. Callens,[a]* C. L'abbé,[a] J. Meersschaut,[a] I. Serdons,[a] W. Sturhahn[b] and T. S. Toellner[b]

[a]Instituut voor Kern- en Stralingsfysica and INPAC, KU Leuven, Celestijnenlaan 200D, B-3001 Leuven, Belgium, and [b]Advanced Photon Source, Argonne National Laboratory, Argonne, IL 60439, USA. E-mail: riet.callens@fys.kuleuven.be

An expression is derived for the line intensities in a nuclear forward-scattering energy spectrum that is obtained *via* a Fourier transformation of the time dependence of the wavefield. The calculation takes into account the coherent properties of the nuclear forward-scattering process and the experimental limitations on the observable time window. It is shown that, for magnetic samples, the spin direction can be determined from the ratios between the different lines in the energy spectrum. The theory is complemented with experimental results on α-iron.

Keywords: magnetometry; Mössbauer; nuclear resonant scattering.

1. Introduction

A challenging problem in magnetism is the selective study of different entities in a magnetic heterostructure as a function of, for example, the external field, the temperature or the shape of the magnetic structure. Mössbauer spectroscopy is an isotope-selective technique and, therefore, allows one to study a particular entity selectively, even when this entity is buried in the material. It provides magnetic information by probing the hyperfine fields. Most Mössbauer experiments are carried out using a radioactive source. However, for the study of samples containing a small amount of the resonant Mössbauer isotope, *e.g.* samples embedded in a high-pressure cell (Mao *et al.*, 2004; Barla *et al.*, 2004, 2005), thin films (Nagy *et al.*, 2002; Röhlsberger *et al.*, 2002, 2004; L'abbé *et al.*, 2004) or nanostructures (Röhlsberger *et al.*, 2001, 2003), the synchrotron source is often a valuable alternative. It has the advantage that it provides a well collimated intense beam. Moreover, the energy of the beam is tunable over a wide range so that many Mössbauer excitations can be accessed (for overviews, see Röhlsberger, 2004; Leupold *et al.*, 1999).

Nuclear resonant scattering experiments with synchrotron radiation are generally performed in a time-differential mode where the nuclear decay is recorded as a function of the time after the excitation by the synchrotron pulse. The quantum beats that are revealed are the fingerprints of the magnetic fields at the position of the Mössbauer nuclei (Trammell & Hannon, 1978; Gerdau *et al.*, 1986). In order to extract the magnetic information from the quantum beat pattern, a substantial effort and experience is required, often inhibiting an on-line interpretation of the data. Therefore, it has been proposed to record both the norm and the phase of the scattered wavefield (Sturhahn, 2001; Sturhahn *et al.*, 2004; Callens *et al.*, 2005), allowing for a Fourier transformation of the wavefield to the energy domain. The obtained spectra are usually less complex and quite easy to interpret. A practical scheme for the phase determination consists of a moving single-line reference sample that is placed in-line with the sample under investigation (Callens *et al.*, 2005). For each nuclear resonant scattered photon, both the time delay and the velocity of the reference sample is recorded. For each time channel, the velocity spectrum is a cosine function, from which the norm and the phase of the wavefield component along the incident polarization can be derived. The energy spectrum is obtained by taking the norm squared of the Fourier-transformed wavefield component.

In Mössbauer spectra taken with a radioactive source, the line intensities depend on the magnetization direction (Frauenfelder *et al.*, 1962; Gonser *et al.*, 1966). In this article we will show that, for an energy spectrum obtained with synchrotron radiation, the magnetization direction can also be determined from the line intensities. Explicit expressions for the line intensities of a ^{57}Fe magnetic spectrum recorded with linearly polarized synchrotron radiation are calculated. The calculation is based on the dynamical theory of nuclear forward scattering (Blume & Kistner, 1968) and takes into account the finite experimental time window. The theory is illustrated by a forward-scattering experiment on an α-iron foil.

2. Calculation of the line intensities

For the calculation of the line intensities in a reconstructed energy spectrum, we will focus on nuclear forward scattering by ^{57}Fe nuclei submitted to a uniaxial magnetic hyperfine field.

The magnetic hyperfine field causes a Zeeman splitting of the nuclear ground and excited states so that several nuclear transitions can be distinguished. For a sufficiently large Zeeman splitting, each allowed transition gives rise to a well resolved resonance line in the energy spectrum. In *Appendix A* we show that, for a sample with Mössbauer thickness L, the intensity of the line associated with the jth hyperfine transition, $P_j(L)$, can be related to the line intensity for a single-line sample, $P_{\rm SL}(W_jL)$, having a weighted Mössbauer thickness W_jL,

$$P_j(L) = P_{\rm SL}(W_j L)|\mathbf{e}_j^* \cdot \mathbf{e}_{\rm in}|^4. \quad (1)$$

The weighting factor W_j depends on the direction of the hyperfine field, the polarization of the incident radiation and the multipolarity of the Mössbauer transition.

The expression $\mathbf{e}_j^* \cdot \mathbf{e}_{\rm in}$ in equation (1) gives the projection of the polarization state of the incident radiation, $\mathbf{e}_{\rm in}$, on the polarization state $\mathbf{e}_j$ of the radiation that is resonantly scattered *via* the jth hyperfine transition. Note that the polarization projection appears to the fourth power in equation (1), owing to the fact that phase reconstruction methods using a single-line reference sample only measure the wavefield component along $\mathbf{e}_{\rm in}$ (Sturhahn *et al.*, 2004; Callens *et al.*, 2005). For the M1 transition in ^{57}Fe and incident radiation that is linearly polarized along $\mathbf{e}_x$, the factors W_j and the polarization projections $|\mathbf{e}_j^* \cdot \mathbf{e}_x|^2$ are given in Table 1.

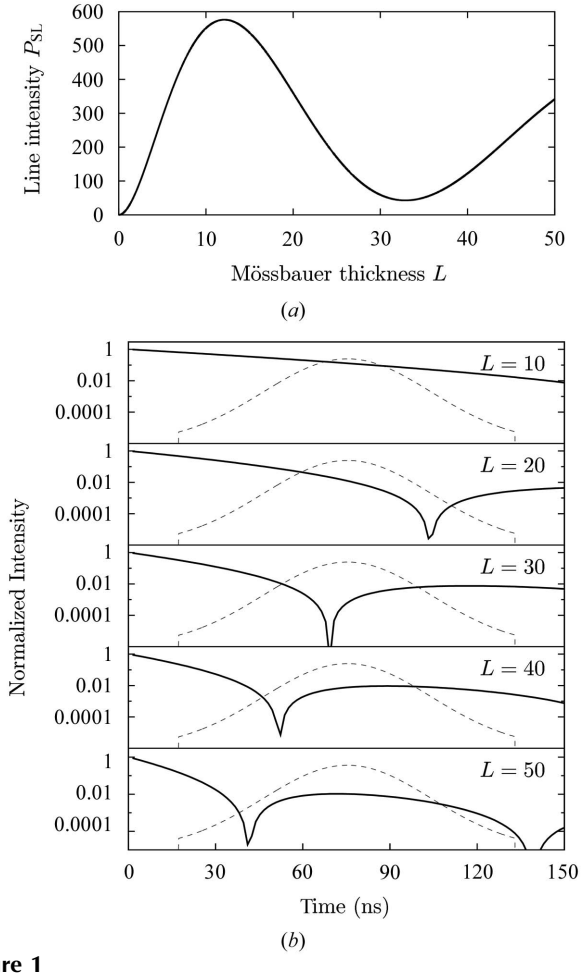

Figure 1
(*a*) Line intensity for a single-line sample as a function of the Mössbauer thickness L for a time window lasting from 17 to 133 ns and a time-window function as defined in equation (2). (*b*) Solid line: time evolution of synchrotron radiation that is nuclear resonant scattered by a single-line sample of Mössbauer thickness L. Dotted line: time-window function as defined in equation (2).

Table 1
The spin projection of the ground state ($m_{\rm g}$) and the excited state ($m_{\rm e}$) on the hyperfine field direction, the thickness weighting factors W_j and the polarization projections $|\mathbf{e}_j^* \cdot \mathbf{e}_x|^2$ for the six allowed transitions in ^{57}Fe.

θ and φ are the polar and the azimuthal angle of the hyperfine field with respect to the propagation direction (z-axis) and the polarization direction (x-axis) of the incident synchrotron radiation, respectively.

j	$m_{\rm g}$	$m_{\rm e}$	W_j	$\lvert\mathbf{e}_j^* \cdot \mathbf{e}_x\rvert^2$
1	−1/2	−3/2	$0.375(1 + \cos^2\theta)$	$(1 - \sin^2\theta\sin^2\varphi)/(1 + \cos^2\theta)$
2	−1/2	−1/2	$0.5\sin^2\theta$	$\sin^2\varphi$
3	−1/2	1/2	$0.125(1 + \cos^2\theta)$	$(1 - \sin^2\theta\sin^2\varphi)/(1 + \cos^2\theta)$
4	1/2	−1/2	$0.125(1 + \cos^2\theta)$	$(1 - \sin^2\theta\sin^2\varphi)/(1 + \cos^2\theta)$
5	1/2	1/2	$0.5\sin^2\theta$	$\sin^2\varphi$
6	1/2	3/2	$0.375(1 + \cos^2\theta)$	$(1 - \sin^2\theta\sin^2\varphi)/(1 + \cos^2\theta)$

Experimentally, the wavefield is measured only in a certain finite time interval. The properties of this experimental time window influence the line intensities. According to equation (1), we can restrict the discussion to the case of a single-line sample. We will work out the example of the time window that was used in the experiment described below, *i.e.* a window lasting from 17 to 133 ns. The energy spectra for single-line samples with different Mössbauer thicknesses are calculated using the procedure outlined in *Appendix A*. In order to reduce truncating wiggles in the energy spectrum, the time dependence of the wavefield is multiplied by a Gaussian before the Fourier transformation is performed. This function is called the time-window function and is given by

$$S(t) = \begin{cases} \exp\left[-(t-75)^2/1682\right] & \text{if } t \in [17; 133] \\ 0 & \text{elsewhere,} \end{cases} \quad (2)$$

where t is in ns. The line intensity $P_{\rm SL}$ is calculated by integrating the energy spectrum over the interval $[\hbar\omega_0 - 3\Gamma; \hbar\omega_0 + 3\Gamma]$ where ω_0 is the resonance frequency and Γ is the natural linewidth of the Mössbauer level. The result is shown in Fig. 1(*a*). In order to intuitively understand this curve, one should have a look at the time dependence of the norm of the forward-scattered wavefield (Fig. 1*b*). If the Mössbauer thickness varies from 10 to 50, the first dynamical minimum is moving through the experimental time window. This explains the maximum around L = 16 and the minimum around L = 33 in the line intensity of Fig. 1(*a*).

An expression for the line-intensity ratios will now be derived from equation (1) and the expressions in Table 1,

$$\frac{P_1}{P_3} = \frac{P_{\rm SL}[0.375(1 + \cos^2\theta)L]}{P_{\rm SL}[0.125(1 + \cos^2\theta)L]}, \quad (3)$$

$$\frac{P_1}{P_2} = \frac{P_{\rm SL}[0.375(1 + \cos^2\theta)L]}{P_{\rm SL}[0.5(\sin^2\theta)L]}\left[\frac{1 - \sin^2\varphi\sin^2\theta}{\sin^2\varphi(1 + \cos^2\theta)}\right]^2. \quad (4)$$

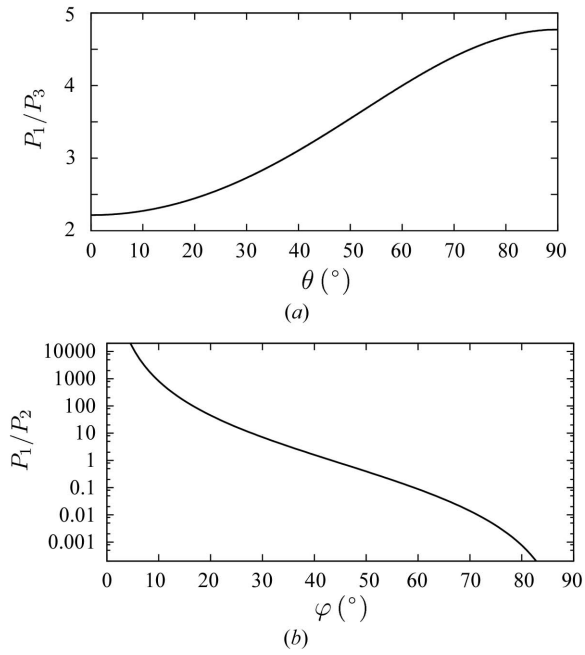

Figure 2
Line-intensity ratios for a Zeeman-split sample with Mössbauer thickness L = 18.2 for the time-window function $S(t)$ of equation (2). (*a*) Dependence of the line-intensity ratio P_1/P_3 on the polar angle θ. (*b*) Dependence of the line-intensity ratio P_1/P_2 on the azimuthal angle φ for $\theta = 90^\circ$.

θ and φ are the polar and the azimuthal angle of the hyperfine field with respect to the propagation direction (z-axis) and the polarization direction (x-axis) of the incident synchrotron radiation. The ratio between the first and the third line [equation (3)] does not depend on the azimuthal angle φ and, therefore, allows one to determine the polar angle θ. Note that, using linearly polarized radiation, one cannot distinguish between a polar angle θ and $180^\circ - \theta$. The degeneracy could be resolved by using circularly polarized radiation (L'abbé *et al.*, 2004). In Fig. 2(*a*) the ratio P_1/P_3 is plotted as a function of the polar angle θ for the experimental time window and the nominal Mössbauer thickness of the sample used in the experiment. The highest sensitivity of the ratio P_1/P_3 to the angle θ is around $\theta = 45^\circ$.

Once the polar angle θ is known, the azimuthal angle φ can be determined from the ratio between the first and the second line [equation (4)]. Again, owing to the $\sin^2$ dependence on the angle φ, different angles give rise to the same line intensities, *i.e.* $\pm\varphi$ and $180^\circ \pm \varphi$. Part of this ambiguity can be resolved by performing a second measurement using a polarizer that tilts the linear polarization direction by 45°. This allows one to distinguish between φ and $180^\circ + \varphi$ on the one hand and $-\varphi$ and $180^\circ - \varphi$ on the other.[1] If the magnetic hyperfine field lies in the plane perpendicular to the propagation direction of the photon, *i.e.* $\theta = 90^\circ$, equation (4) can be rewritten as

$$\frac{P_1}{P_2} = \frac{P_{\rm SL}(0.375L)}{P_{\rm SL}(0.5L)} \frac{1}{\tan^4 \varphi}. \qquad (5)$$

This function is plotted in Fig. 2(*b*) for the nominal Mössbauer thickness of the sample used in the experiment. Since the intensity of either the first or the second line is negligible near $\varphi = 90^\circ$ or $\varphi = 0^\circ$, respectively, optimal sensitivity is achieved in the intermediate region. Note that performing a second measurement using a polarizer that tilts the linear polarization direction by 45° will improve the sensitivity near $\varphi = 90^\circ$ and $\varphi = 0^\circ$.

3. Experimental results

The formalism will be illustrated using experimental data on an α-iron foil. The experiment was performed at the Advanced Photon Source at beamline XOR-3-ID (Alp *et al.*, 1994), a beamline that is specially designed for nuclear resonant scattering experiments. The ring was operated in the standard top-up mode consisting of singlets with 153 ns interval. The energy of the beam was tuned to the 14.4 keV Mössbauer transition in ^{57}Fe. In order to filter a 1 meV bandwidth, a high-resolution monochromator consisting of a pair of asymmetrically cut silicon (4 0 0) reflections followed by a pair of asymmetrically cut silicon (10 6 4) reflections was used (Toellner, 2000). The polarization of the beam is known to lie in the plane of the storage ring. The sample was a 50 µm-thick natural α-iron foil. It was placed perpendicular to the beam and magnetized along four different directions in the plane of the foil ($\theta = 90^\circ$) using a small external field. For the energy-resolved measurements, a 95% ^{57}Fe-enriched stainless-steel reference foil was placed in line with the α-iron foil. The foil was mounted on a velocity drive operating in the sinusoidal mode with a maximum velocity of 16.7 mm s^{-1}. For the photons with a delay between 17 and 133 ns, both the time delay and the velocity of the reference sample were registered. Using the computer code *PHASE*,[2] the data were transformed to the energy spectra of Fig. 3(*a*). This code was developed to automatically perform the procedure outlined by Callens *et al.* (2005). It does not require any information on the sample parameters and can be used for on-line visualization of the data.

The energy spectra of Fig. 3(*a*) provide us directly with information about the direction of the magnetic hyperfine field. Assuming that the magnetic hyperfine field lies in the plane of the foil, *i.e.* $\theta = 90^\circ$, we can use equation (5) for the determination of the azimuthal angle φ. The experimental line-intensity ratios P_1/P_2 and the values for the azimuthal angle φ_p derived from these ratios are tabulated in Table 2. These values are in good agreement with the values φ_t obtained from a *CONUSS* (Sturhahn, 2000) analysis of time spectra taken without reference sample in the beam (Fig. 3*b*). The polar angle θ can also be derived from the experimental energy spectra. We find that the line-intensity ratio $P_1/P_3 \geq$

[1] In order to calculate the line-intensity ratios for the set-up with the polarizer tilted by 45°, the angle φ in equation (4) should be replaced by $\varphi - 45^\circ$.

[2] On request, the computer code *PHASE* is available from the author.

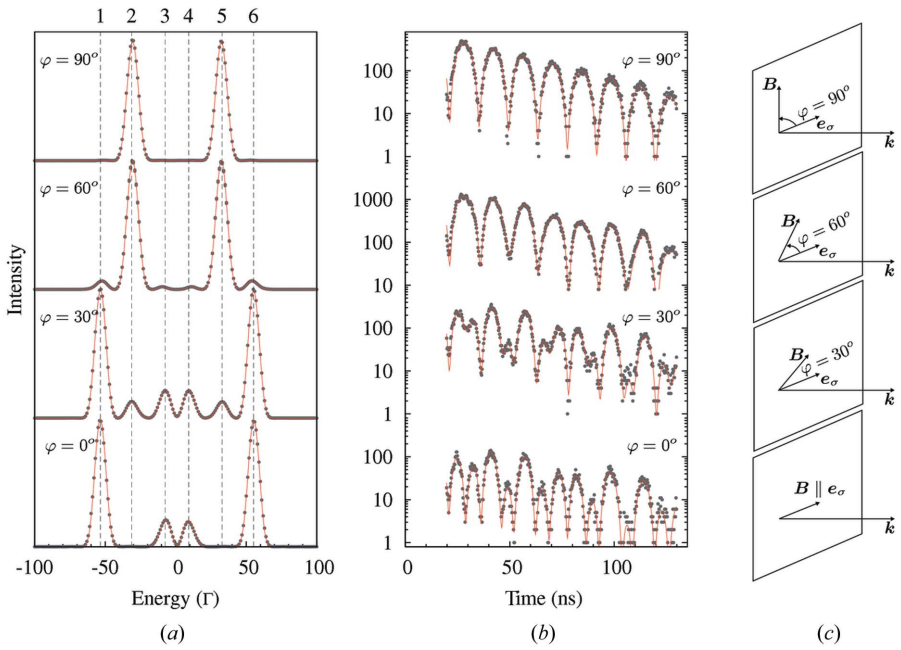

Figure 3
Nuclear resonant scattering data for an α-iron foil with the hyperfine field **B** oriented along different directions in the plane perpendicular to the photon direction **k** ($\theta = 90^\circ$). The angle φ is the angle between the polarization of the radiation $\mathbf{e}_x$ and the direction of the magnetic hyperfine field **B**. The dots are the data and the solid line is a fit obtained using the software package *CONUSS* (Sturhahn, 2000). (*a*) Energy spectra. The energy scale is given in units of the natural linewidth of the Mössbauer level in ^{57}Fe, $\gamma = 4.66$ neV. (*b*) Time spectra taken without reference sample in the beam. (*c*) Schematic picture of the hyperfine field direction with respect to the photon direction.

Table 2
The line-intensity ratio P_1/P_2 calculated from the experimental energy spectra of Fig. 3(*a*), the azimuthal angle φ_p deduced from this ratio, and the azimuthal angle φ_t determined from the *CONUSS* analysis of the time spectra of Fig. 3(*b*).

φ (°)	P_1/P_2	φ_p (°)	φ_t (°)
90	<0.0035	83 (7)	84 (4)
60	0.0659	62 (1)	62 (2)
30	7.78	29 (1)	28 (2)
0	>400	7 (7)	2 (3)

4.7, from which we can conclude that $\theta = 84\ (6)^\circ$. In order to determine the azimuthal angle φ using $\theta = 84\ (6)^\circ$, the more general expression of equation (4) was used. Within the error bars, we found the same results as for $\theta = 90^\circ$.

4. Conclusion

From the line-intensity ratios in the reconstructed energy spectrum, the magnetization direction can be deduced. For incident synchrotron light that is linearly polarized, the polar angle θ can be determined from the intensity ratio between the first and the third line. This determination is most sensitive around 45°. Once the polar angle θ is known, the azimuthal angle φ is obtained from the intensity ratio between the first and the second line. Also, for the azimuthal angle φ, the highest sensitivity is obtained around 45°.

APPENDIX *A*
Detailed calculation of the line intensity

In the following, an expression for the line intensities in a nuclear forward-scattering energy spectrum of a ^{57}Fe Zeeman-split sample is derived. The magnetic hyperfine field is assumed to be uniaxial and sufficiently large so that the lines in the spectrum are completely resolved. The energy dependence of the wavefield transmitted through the sample in the vicinity of the nuclear transition frequency ω_j equals (Blume & Kistner, 1968)

$$\mathbf{E}_{\rm tr}(\omega-\omega_j) = \exp\left[i(2\pi/k)\rho f(\omega-\omega_j)d\right] \times \mathbf{E}_{\rm in}, \quad (6)$$

where k is the wavenumber, ρ is the concentration of the chemical element, f is the coherent forward-scattering matrix from a single nucleus, d is the sample thickness and $\mathbf{E}_{\rm in} = E_{\rm in}\mathbf{e}_{\rm in}$ is the incoming wavefield polarized along $\mathbf{e}_{\rm in}$. For a single-line sample with resonance frequency ω_j, the matrix f is a diagonal matrix explicitly given by (Hannon & Trammell, 1969)

$$f(\omega-\omega_j) = -\frac{k}{8\pi}\sigma_0 f_{LM}\,\chi\frac{\gamma}{\omega-\omega_j+i\gamma/2}\begin{bmatrix}1 & 0\\ 0 & 1\end{bmatrix}, \quad (7)$$

where γ is the inverse of the lifetime of the excited state, f_{LM} is the recoilless fraction, χ is the isotopic enrichment and σ_0 is the maximal resonant-scattering cross section. By combining equations (6) and (7) we find that the wavefield transmitted through a single-line sample is given by

$$\mathbf{E}_{\rm SL}(\omega-\omega_j, L) = \exp\left(-i\,\frac{L}{4}\frac{\gamma}{\omega-\omega_j+i\gamma/2}\right)E_{\rm in}\mathbf{e}_{\rm in}, \quad (8)$$

where the Mössbauer thickness L is defined as

$$L = \sigma_0 f_{LM}\,\chi\rho d. \quad (9)$$

In the case of a hyperfine-split sample, there are several resonance frequencies ω_j. For well separated hyperfine levels, the matrix for coherent scattering by a single ^{57}Fe nucleus in the vicinity of a transition frequency ω_j is given by (Hannon & Trammell, 1969)

$$f(\omega-\omega_j) = -\frac{k}{8\pi}\sigma_0 f_{LM}\,\chi\,\frac{3}{4}C_j^2\,\zeta_{1M}\,\frac{\gamma}{\omega-\omega_j+i\gamma/2}, \quad (10)$$

where C_j is the Clebsch–Gordan coefficient,

$$C_j = C\left(\tfrac{1}{2}\ 1\ \tfrac{3}{2};\ m_g\ M\ m_e\right),$$

in the notation of Rose (1957) and is given in Table 3. The matrix ζ_{1M} gives the dependence of the scattering matrix on the direction of the hyperfine field. It is defined in terms of

Table 3
The spin projection of the ground state (m_g) and the excited state (m_e) on the hyperfine field direction, the change in spin projection (M), the square of the Clebsch–Gordan coefficients (C_j^2), the eigenvalues λ_j, and the projections $\mathbf{e}_+^* \cdot \mathbf{e}_j$ and $\mathbf{e}_-^* \cdot \mathbf{e}_j$ for the six allowed transitions in ^{57}Fe.

θ and φ are the polar and the azimuthal angle of the hyperfine field with respect to the propagation direction (z-axis) and the polarization direction (x-axis) of the incident synchrotron radiation.

j	m_g	m_e	M	C_j^2	λ_j	$\mathbf{e}_+^* \cdot \mathbf{e}_j$	$\mathbf{e}_-^* \cdot \mathbf{e}_j$
1	−1/2	−3/2	−1	1	$(1+\cos^2\theta)/2$	$\sqrt{2}\sin^2(\theta/2)/\sqrt{1+\cos^2\theta}$	$-\sqrt{2}\exp(-2i\varphi)\cos^2(\theta/2)/\sqrt{1+\cos^2\theta}$
2	−1/2	−1/2	0	2/3	$\sin^2\theta$	$1/\sqrt{2}$	$\exp(-2i\varphi)/\sqrt{2}$
3	−1/2	1/2	+1	1/3	$(1+\cos^2\theta)/2$	$\sqrt{2}\cos^2(\theta/2)/\sqrt{1+\cos^2\theta}$	$-\sqrt{2}\exp(-2i\varphi)\sin^2(\theta/2)/\sqrt{1+\cos^2\theta}$
4	1/2	−1/2	−1	1/3	$(1+\cos^2\theta)/2$	$\sqrt{2}\sin^2(\theta/2)/\sqrt{1+\cos^2\theta}$	$-\sqrt{2}\exp(-2i\varphi)\cos^2(\theta/2)/\sqrt{1+\cos^2\theta}$
5	1/2	1/2	0	2/3	$\sin^2\theta$	$1/\sqrt{2}$	$\exp(-2i\varphi)/\sqrt{2}$
6	1/2	3/2	+1	1	$(1+\cos^2\theta)/2$	$\sqrt{2}\cos^2(\theta/2)/\sqrt{1+\cos^2\theta}$	$-\sqrt{2}\exp(-2i\varphi)\sin^2(\theta/2)/\sqrt{1+\cos^2\theta}$

Table 4
The matrix elements of ζ_{1M} in the basis of circular polarization ($\mathbf{e}_+$, $\mathbf{e}_-$).

θ and φ are the polar and the azimuthal angle of the hyperfine field with respect to the propagation direction (z-axis) and the polarization direction (x-axis) of the incident synchrotron radiation.

	$\mathbf{e}_{sc}\mathbf{e}_{in} = \mathbf{e}_+\mathbf{e}_+$	$\mathbf{e}_{sc}\mathbf{e}_{in} = \mathbf{e}_+\mathbf{e}_-$	$\mathbf{e}_{sc}\mathbf{e}_{in} = \mathbf{e}_-\mathbf{e}_+$	$\mathbf{e}_{sc}\mathbf{e}_{in} = \mathbf{e}_-\mathbf{e}_-$
$M = +1$	$[(1+\cos\theta)/2]^2$	$-\frac{1}{4}\sin^2\theta\exp(2i\varphi)$	$-\frac{1}{4}\sin^2\theta\exp(-2i\varphi)$	$[(1-\cos\theta)/2]^2$
$M = 0$	$\frac{1}{2}\sin^2\theta$	$\frac{1}{2}\sin^2\theta\exp(2i\varphi)$	$\frac{1}{2}\sin^2\theta\exp(-2i\varphi)$	$\frac{1}{2}\sin^2\theta$
$M = -1$	$[(1-\cos\theta)/2]^2$	$-\frac{1}{4}\sin^2\theta\exp(2i\varphi)$	$-\frac{1}{4}\sin^2\theta\exp(-2i\varphi)$	$[(1+\cos\theta)/2]^2$

the vector spherical harmonics $\mathbf{Y}_{1M}^{(1)}(\mathbf{k})$ and the polarization vectors $\mathbf{e}_{in}$ and $\mathbf{e}_{sc}$ before and after the scattering process,

$$\zeta_{1M} = 8\pi \mathbf{e}_{sc}^* \cdot \mathbf{Y}_{1M}^{(1)}(\mathbf{k})\mathbf{Y}_{1M}^{(1)}(\mathbf{k})^* \cdot \mathbf{e}_{in}. \quad (11)$$

The matrix elements in the basis of circular polarization are listed in Table 4. The eigenvalues of this matrix are calculated according to equation (59) in Hannon & Trammell (1969) and are given by λ_j (Table 3) and 0, resulting in the following expression for the matrix ζ_{1M} in the eigenbasis of the jth transition,

$$\zeta_{1M} = \begin{bmatrix} \lambda_j & 0 \\ 0 & 0 \end{bmatrix}. \quad (12)$$

Combining equations (6), (10) and (12) yields an expression for the transmitted wavefield in the vicinity of the transition frequency ω_j,

$$\mathbf{E}_j(\omega-\omega_j, L) = \exp\left[-i\frac{W_j L}{4}\frac{\gamma}{\omega-\omega_j+i\gamma/2}\right]E_{in}(\mathbf{e}_j^*\cdot\mathbf{e}_{in})\mathbf{e}_j, \quad (13)$$

where W_j is defined as

$$W_j = \frac{3}{4}C_j^2\lambda_j \quad (14)$$

and $\mathbf{e}_j$ is the eigenpolarization corresponding to λ_j. Explicit expressions for $\mathbf{e}_j$ in the basis of circular polarization can be calculated using equation (60) of Hannon & Trammell (1969), and are tabulated in Table 3. Expressions for $|\mathbf{e}_j^*\cdot\mathbf{e}_{in}|^2$ for the case of incident linearly polarized radiation $\mathbf{e}_{in} = \mathbf{e}_x = 2^{-1/2}(-\mathbf{e}_+ + \mathbf{e}_-)$ are given in Table 1.

If we compare the argument of the exponential function in equation (13) with that for the single-line sample in equation (8), we find that they are identical except for the Mössbauer thickness that is scaled with the factor W_j. Consequently, the transmitted wavefield for a particular nuclear transition can be written as

$$\mathbf{E}_j(\omega-\omega_j, L) = E_{SL}(\omega-\omega_j, W_j L)(\mathbf{e}_j^*\cdot\mathbf{e}_{in})\mathbf{e}_j. \quad (15)$$

Using the phase determination method described by Callens *et al.* (2005), the component along $\mathbf{e}_{in}$ of this wavefield is measured,

$$\begin{aligned} E_j^{in}(\omega-\omega_j, L) &= \mathbf{e}_{in}^*\cdot\mathbf{E}_j(\omega-\omega_j, L) \\ &= E_{SL}(\omega-\omega_j, W_j L)\,|\mathbf{e}_j^*\cdot\mathbf{e}_{in}|^2. \end{aligned} \quad (16)$$

Since the intensity is proportional to the square of the norm of the wavefield, the line intensity for the jth resonance is given by

$$P_j(L) = P_{SL}(W_j L)|\mathbf{e}_j^*\cdot\mathbf{e}_{in}|^4, \quad (17)$$

where $P_{SL}(W_j L)$ is the line intensity for a single-line sample having a Mössbauer thickness $W_j L$.

For the calculation of the line intensity $P_{SL}(W_j L)$ for a single-line sample, one has to take into account the experimental time-window. The time dependence of the nuclear resonant wavefield for a single-line sample with Mössbauer thickness L and resonance frequency ω_j is given by (Kagan *et al.*, 1979)

$$\mathbf{E}_{SL}(t, \omega_j, L) \simeq \begin{cases} -L\exp[-i\omega_j t - (t/2\tau)]J_1[(Lt/\tau)^{1/2}]\mathbf{e}_{in}/(Lt/\tau)^{1/2} & \text{if } t \geq 0 \\ 0 & \text{if } t < 0, \end{cases} \quad (18)$$

where τ is the lifetime of the Mössbauer level and J_1 is the first-order Bessel function. This expression for the wavefield is multiplied by the experimental time-window function $S(t)$ and Fourier transformed to the energy domain,

$$\mathbf{E}_{SL}^S(\omega-\omega_j, L) \simeq \int_{-\infty}^{+\infty} dt\, \exp[-i(\omega-\omega_j)t]S(t)E_{SL}(t, \omega_j, L)\mathbf{e}_{in}. \quad (19)$$

The norm squared of this wavefield corresponds to the intensity in the energy domain. As a measure for the line intensity, we will integrate the intensity over the interval $[\omega_j - 3\gamma; \omega_j + 3\gamma]$ where $\gamma = 1/\tau$ is the inverse of the lifetime.

Thus, the expression for the line intensity for a single-line sample is given by

$$P_{\rm SL}(L) \simeq \int_{\omega_j-3\gamma}^{\omega_j+3\gamma} {\rm d}\omega \, |E^S_{\rm SL}(\omega-\omega_j, L)|^2. \qquad (20)$$

Equations (17)–(20) now allow for the calculation of the line-intensity ratios as a function of the direction of the hyperfine field (see §2).

This work was supported by the Fund for Scientific Research-Flanders (G.0224.02 and G.0498.04), the Inter-University Attraction Pole (IUAP P5/1), the Concerted Action of the KULeuven (GOA/2004/02), the Centers of Excellence Programme INPAC EF/05/005 and by the European Community *via* STREP No. NMP4-CT-2003-001516 (DYNASYNC). Use of the Advanced Photon Source was supported by the US DOE, Office of Science, under Contract No. W-31-109-Eng-38. RC and CL'a thank the FWO-Flanders for financial support.

References

Alp, E. E., Mooney, T. M., Toellner, T. & Sturhahn, W. (1994). *Hyperfine Interact.* **90**, 323–334.

Barla, A., Derr, J., Sanchez, J. P., Salce, B., Lapertot, G., Doyle, B. P., Rüffer, R., Lengsdorf, R., Abd-Elmeguid, M. M. & Flouquet, J. (2005). *Phys. Rev. Lett.* **94**, 166401.

Barla, A., Sanchez, J. P., Haga, Y., Lapertot, G., Doyle, B. P., Leupold, O., Rüffer, R., Abd-Elmeguid, M. M., Lengsdorf, R. & Flouquet, J. (2004). *Phys. Rev. Lett.* **92**, 066401.

Blume, M. & Kistner, O. C. (1968). *Phys. Rev.* **171**, 417–425.

Callens, R., L'abbé, C., Meersschaut, J., Serdons, I., Sturhahn, W. & Toellner, T. S. (2005). *Phys. Rev. B*, **72**, 081402(R).

Frauenfelder, H., Nagle, D. E., Taylor, R. D., Cochran, D. R. F. & Visscher, W. M. (1962). *Phys. Rev.* **126**, 1065–1075.

Gerdau, E., Rüffer, R., Hollatz, R. & Hannon, J. P. (1986). *Phys. Rev. Lett.* **57**, 1141–1144.

Gonser, U., Grant, R. W., Wiedersich, H. & Geller, S. (1966). *Appl. Phys. Lett.* **9**, 18–21.

Hannon, J. P. & Trammell, G. T. (1969). *Phys. Rev.* **186**, 306–325.

Kagan, Y., Afanas'ev, A. M. & Kohn, V. G. (1979). *J. Phys. C*, **12**, 615–631.

L'abbé, C., Meersschaut, J., Sturhahn, W., Jiang, J. S., Toellner, T. S., Alp, E. E. & Bader, S. D. (2004). *Phys. Rev. Lett.* **93**, 037201.

Leupold, O., Chumakov, A. I., Alp, E. E., Sturhahn, W. & Baron, A. Q. R. (1999). *Hyperfine Interact.* **123**, 611–631.

Mao, W. L., Sturhahn, W., Heinz, D. L., Mao, H. K., Shu, J. F. & Hemley, R. J. (2004). *Geophys. Res. Lett.* **31**, L15618.

Nagy, D. L., Bottyan, L., Croonenborghs, B., Deak, L., Degroote, B., Dekoster, J., Lauter, H. J., Lauter-Pasyuk, V., Leupold, O., Major, M., Meersschaut, J., Nikonov, O., Petrenko, A., Rüffer, R., Spiering, H. & Szilagyi, E. (2002). *Phys. Rev. Lett.* **88**, 157202.

Röhlsberger, R. (2004). *Nuclear Condensed Matter Physics with Synchrotron Radiation: Basic Principles, Methodology and Applications.* Berlin: Springer.

Röhlsberger, R., Bansmann, J., Senz, V., Jonas, K. L., Bettac, A., Leupold, O., Rüffer, R., Burkel, E. & Meiwes-Broer, K. H. (2001). *Phys. Rev. Lett.* **86**, 5597–5600.

Röhlsberger, R., Bansmann, J., Senz, V., Jonas, K. L., Bettac, A., Meiwes-Broer, K. H. & Leupold, O. (2003). *Phys. Rev. B*, **67**, 245412.

Röhlsberger, R., Klein, T., Schlage, K., Leupold, O. & Rüffer, R. (2004). *Phys. Rev. B*, **69**, 235412.

Röhlsberger, R., Thomas, H., Schlage, K., Burkel, E., Leupold, O. & Rüffer, R. (2002). *Phys. Rev. Lett.* **89**, 237201.

Rose, M. E. (1957). *Elementary Theory of Angular Momentum.* New York: John Wiley and Sons.

Sturhahn, W. (2000). *Hyperfine Interact.* **125**, 149–172.

Sturhahn, W. (2001). *Phys. Rev. B*, **63**, 094105.

Sturhahn, W., L'abbé, C. & Toellner, T. S. (2004). *Europhys. Lett.* **66**, 506–512.

Toellner, T. S. (2000). *Hyperfine Interact.* **125**, 3–28.

Trammell, G. T. & Hannon, J. P. (1978). *Phys. Rev. B*, **18**, 165–172. [Erratum: *Phys. Rev. B*, (1979). **19**, 3835–3836.]